中島孝	患者の病態にあわせて適切なバリエーションを選択—ガイドラインの作成の実際の適応	難病と在宅ケア	Vol.14(2)	9-12	2008
宮下光令、秋山美紀、落合亮太、萩原章子、中島孝、福原俊一、大生定義	神経内科的疾患患者の在宅介護者に対する「個別化された重みつきQOL尺度」SEIQoL-DWの測定	厚生の指標	55(1)	9-14	2008
中島孝	QOLと緩和ケアの奪還	現代思想	Vol.36:2	148-173	2008
中島孝、伊藤博明	緩和ケアとは本来何なのか？生きるためのケアにむけて	難病と在宅ケア	Vol. 13(10)	9-13	2008
中島孝	神経難病と音楽療法　総論	神経内科	67(3)	228-235	2007

IV. 研究成果の刊行物・別刷

Eur J Nucl Med Mol Imaging
DOI 10.1007/s00259-007-0654-4

ORIGINAL ARTICLE

Absolute quantitation of myocardial blood flow with ^{201}Tl and dynamic SPECT in canine: optimisation and validation of kinetic modelling

Hidehiro Iida · Stefan Eberl · Kyeong-Min Kim · Yoshikazu Tamura · Yukihiko Ono · Mayumi Nakazawa · Antti Sohlberg · Tsutomu Zeniya · Takuya Hayashi · Hiroshi Watabe

Received: 18 September 2007 / Accepted: 4 November 2007

Abstract
Purpose ^{201}Tl has been extensively used for myocardial perfusion and viability assessment. Unlike ^{99m}Tc-labelled agents, such as ^{99m}Tc-sestamibi and ^{99m}Tc-tetrofosmine, the regional concentration of ^{201}Tl varies with time. This study is intended to validate a kinetic modelling approach for in vivo quantitative estimation of regional myocardial blood flow (MBF) and volume of distribution of ^{201}Tl using dynamic SPECT.
Methods Dynamic SPECT was carried out on 20 normal canines after the intravenous administration of ^{201}Tl using a commercial SPECT system. Seven animals were studied at rest, nine during adenosine infusion, and four after beta-blocker administration. Quantitative images were reconstructed with a previously validated technique, employing OS-EM with attenuation-correction, and transmission-dependent convolution subtraction scatter correction. Measured regional time–activity curves in myocardial segments were fitted to two- and three-compartment models. Regional MBF was defined as the influx rate constant (K_1) with corrections for the partial volume effect, haematocrit and limited first-pass extraction fraction, and was compared with that determined from radio-labelled microspheres experiments.
Results Regional time–activity curves responded well to pharmacological stress. Quantitative MBF values were higher with adenosine and decreased after beta-blocker compared to a resting condition. MBFs obtained with SPECT (MBF_{SPECT}) correlated well with the MBF values obtained by the radio-labelled microspheres (MBF_{MS}) ($MBF_{SPECT}=-0.067+1.042\times MBF_{MS}$, $p<0.001$). The three-compartment model provided better fit than the two-compartment model, but the difference in MBF values between the two methods was small and could be accounted for with a simple linear regression.
Conclusion Absolute quantitation of regional MBF, for a wide physiological flow range, appears to be feasible using ^{201}Tl and dynamic SPECT.

Keywords Myocardial blood flow · Dynamic SPECT · Thallium-201 · Compartment model · Quantitation

H. Iida (✉) · S. Eberl · K.-M. Kim · M. Nakazawa · A. Sohlberg · T. Zeniya · T. Hayashi · H. Watabe
Department of Investigative Radiology,
National Cardiovascular Center Research Institute,
Fujishiro-dai,
Suita City, Osaka 565-8565, Japan
e-mail: iida@ri.ncvc.go.jp

S. Eberl
PET and Nuclear Medicine Department,
Royal Prince Alfred Hospital,
Missenden Road,
Camperdown, NSW 2050, Australia

Y. Tamura
Department of Cardiology, Akita Kumiai General Hospital,
1-1-1, Nishi-bukuro, Iijima,
Akita City 011-0948, Japan

Y. Ono
Akita Research Institute of Brain,
6-10, Senshu-Kubota Machi,
Akita City 010-0874, Japan

Introduction

Myocardial perfusion imaging using Thallium-201 (^{201}Tl) is well established in routine clinical practice for detecting

exercise-induced myocardial ischaemia and/or for assessing myocardial viability in patients with coronary artery disease. The diagnosis, however, has been limited to qualitative or visual assessment of the physical extent of the defect areas rather than quantitative assessment of physiological functions. Quantitative methods would for example enable longitudinal studies when assessing therapy response and pharmacological interventions. Some groups have already investigated the feasibility of estimating quantitative parameters with dynamic SPECT in the myocardium using ^{201}Tl [1] and ^{99m}Tc-Teboroxime [1, 2], but these techniques have not yet been applied to clinical practice. This is largely attributed to the fact that quantitative reconstruction programmes are not readily available on commercial SPECT systems.

We have developed a reconstruction programme package for SPECT, which can accurately provide quantitative images of radio-labelled tracer distributions in vivo, which is a pre-requisite for absolute physiological parameter estimation. The adequacy and accuracy of these methods have been demonstrated in multiple papers for ^{99m}Tc and ^{201}Tl in cardiac studies [3–5], and for ^{99m}Tc and ^{123}I in brain studies [6]. It has also been demonstrated, in brain studies, that physiological parameters such as cerebral perfusion [6] and cerebral flow reactivity [7] obtained using our package were as accurate as those determined by PET. These findings suggest that absolute quantitation of regional myocardial perfusion might also be possible in a clinical setting using commercial SPECT cameras.

^{201}Tl is a potassium analogue, and its kinetics has been extensively investigated in previous studies [8, 9]. Due to the high first-pass extraction fraction (EF) [10] and a large distribution volume, ^{201}Tl has been considered an ideal tracer for quantitation of absolute myocardial blood flow, not only at rest but also at hyperemic conditions. As a clinical implication, quantitative assessment of MBF and coronary flow reserve is important. For instance, coronary microvascular dysfunction or impaired endothelial function in patients with coronary risk factors or patients with cardiomyopathy or with heart failure is an un-resolved important issue to answer [11]. Coronary flow reserve can also be reduced in patients with hyper-cholesterolemia without overt coronary stenosis [12]. The low energy and long half-life of ^{201}Tl have, however, seriously limited its use in nuclear cardiology.

The goal of this study was to validate our reconstruction methodology for the estimation of myocardial blood flow using ^{201}Tl and dynamic SPECT using tissue time–activity curves (TTAC) derived from myocardial regions. In addition, we aimed to find the optimal kinetic model configuration and to investigate the factors affecting the estimation of physiological parameters such as the partial volume effect (PVE), appropriate choice of input function, conversion from plasma to blood flow using haematocrit (Hct) and the limited first-pass tracer EF.

Materials and methods

Subjects

A total of 21 dogs were studied in which 8 were in a resting condition, 9 dogs during constant infusion of adenosine for increased MBF, and 4 dogs during constant infusion of beta-blocker. Of the 21 studies, 1 study was un-successful and projection data could not be retrieved from the scanner, reducing the number of resting studies to 7 and total dog studies to 20. Adenosine was infused continuously over the study duration at a rate ranging from 140 to 700 mg/kg/h to achieve a range of blood flow increases. An initial dose of beta-blockers ranging from 2 to 6 mg was given, followed by a constant infusion for the duration of the study of 2 or 4 mg/h. The study protocol was approved by the animal ethics committee at the Akita Research Institute of Brain, Akita City, Japan where all experiments were carried out.

SPECT procedures

All dogs were anaesthetised, and the catheters for dose administration and arterial blood sampling were inserted before the study. The SPECT system was a conventional dual-head gamma camera (Toshiba GCA-7200A, Tokyo, Japan) fitted with short focal length fan-beam collimators (LEHR-Fan). The transverse field-of-view (FOV) was 22 cm diameter and axial FOV was 20 cm. The dogs were carefully taped into a cradle to minimise motion during the study, and also to ensure that no truncation occurred. Heart rate and blood pressure were monitored throughout the study and recorded at regular intervals.

Before the injection of any tracer, a 15-min transmission study was carried out in which a rod source filled with approximately 740 MBq of ^{99m}Tc was placed along the focal line of one of the fan-beam collimators (see Fig. 1). The transmission study was followed by injection of 3 MBq of ^{141}Ce microspheres into the left ventricle via a catheter and blood was withdrawn from the aorta at a constant flow rate of 5 ml/min for 2 min to serve as an input function. For the pharmacological intervention studies, adenosine infusion or beta-blocker injection followed by infusion was commenced before the ^{141}Ce microsphere administration.

Dynamic SPECT was commenced with the start of the 4-min constant infusion of 110 MBq ^{201}Tl. The frame collection rates and 360° rotation times were 10×1 min (rotation time 15 s), 6×2 min (30 s), 3×4 min (60 s) and 5×5 min (60 s) for the first hour for all studies. Resting blood flow studies had an additional 18×10 min (120 s) frames collected for a total study period over 4 h. The shorter total study time for the drug infusion studies was mandated by the difficulties in keeping the dogs stable with prolonged infusions of the drugs used. A 34% energy

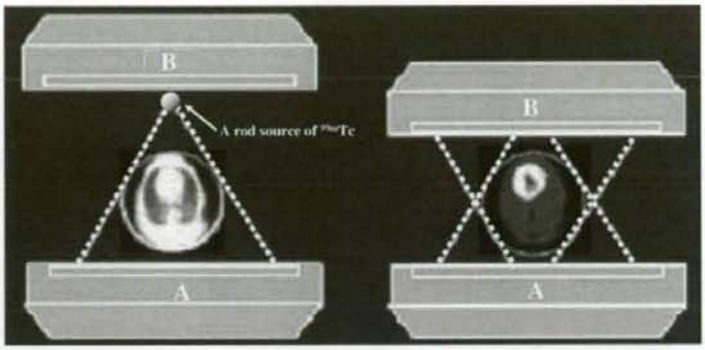

Fig. 1 Schematic diagram of data acquisition using a clinical dual-headed SPECT camera fitted with fan-beam collimators. Transmission scan was performed using a ^{99m}Tc-filled rod source placed at a focal line of one of the collimators, and only one of the detectors was used (*left*). Both detectors were used in the emission scan (*right*)

window centred on 77 keV was used for the ^{201}Tl acquisitions [4, 13].

Arterial blood samples were taken every 20 s for the first 6 min, every 60 s for 6–10 min, 120 s for 10–20 min, 300 s for 20–30 min and 600 s for 30–60 min. For the resting studies, blood samples were also taken every 20 min for 1–2 h and additional samples at 2.5, 3 and 4 h post-^{201}Tl infusion. In six studies, plasma was separated immediately after sampling by centrifugation, and plasma samples were counted in a well counter cross-calibrated with the SPECT scanner. To minimise the effects of the continued exchange of ^{201}Tl between plasma and red blood cells in the test tubes after sampling, immediate, rapid separation of plasma from whole blood was required. An averaged relationship between plasma and whole blood concentration ratio over time was obtained, and then multiplied with the whole blood curves for all studies to derive a plasma input function.

At the end of the SPECT study, the microsphere blood flow measurement was repeated with ^{51}Cr microspheres. The dogs were then killed by injection of potassium chloride (KCl) and the myocardium was dissected into samples suitable for counting in the well counter. The ^{201}Tl concentration in the tissue samples was derived from the sample weight normalised gamma counter counts. The samples were stored to allow for the decay of ^{201}Tl ($T_{1/2}$= 73 h vs $T_{1/2}$=32.5 days for ^{141}Ce and 27.8 days for ^{51}Cr) and then counted to measure the ^{141}Ce and ^{51}Cr activities. Separation between ^{141}Ce and ^{51}Cr counts was based on their respective gamma ray energies (145 keV for ^{141}Ce and 323 keV for ^{51}Cr).

SPECT data processing

Projection data were processed according to previously described procedures [5]. Briefly, the transmission data obtained by the fan-beam collimator were first re-binned into parallel projections. Transmission projections were normalised by blank projection, re-constructed to generate quantitative maps of the attenuation coefficient for ^{99m}Tc and then linearly scaled to provide attenuation correction maps for ^{201}Tl. Emission data were corrected for detector non-uniformity and also re-binned into parallel projections. The projection data were then corrected for scatter with transmission-dependent convolution subtraction (TDCS) originally proposed by Meikle et al. [14] and further optimised by our group [4, 5]. The emission projection data were re-constructed with the OS-EM reconstruction algorithm [15] using three iterations and ten subsets. The re-constructed images were cross-calibrated with the well counter system.

Data analysis

Re-constructed images were normalised by acquisition time for each frame. Multiple circular regions of interest (ROI) were drawn on the myocardium, and the TTAC of ^{201}Tl were generated for the anterior, apical, lateral, posterior and septal areas of the myocardium. The two-compartment model (one tissue compartment) and three-compartment model (two tissue compartments) shown in Fig. 2 were applied to determine two parameters (K_1 and K_2) for the two-compartment model and four parameters (K_1–K_4) for the three-compartment model by means of non-linear least squares fitting (NLLSF).

The regional MBF was considered to be related to K_1 obtained from compartment model fits. K_1 is, however, affected by the PVE, Hct and the limited first-pass EF whose effects were corrected according to Eq. 1:

$$\mathrm{MBF} = \frac{\mathrm{PVE}}{\mathrm{EF} \times (1 - \mathrm{Hct})} \times K_1 \quad (1)$$

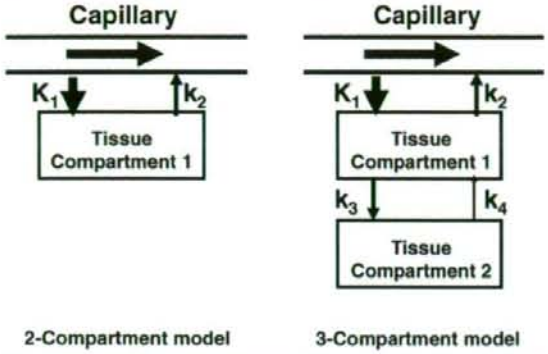

Fig. 2 Two- and three-compartment models evaluated in this study. K_1 in units of ml/min/g denotes the regional MBF for both models. Distribution volume (V_d) in units of ml/g is defined as K_1/k_2 for the two-compartment mode, and $\frac{K_1}{k_2}\left(1+\frac{k_3}{k_4}\right)$ for the three-compartment model

The physiological basis for the correction factors in Eq. 1 can be described as follows:

1. TTACs obtained from SPECT images are under-estimated due to the limited spatial resolution relative to the myocardial wall thickness and also due the myocardial contractile motion. This phenomenon is known as PVE. The PVE correction factor for each TTAC was determined from the ratio of the last SPECT frame counts to the ^{201}Tl myocardial tissue sample counts obtained from the tissue samples taken and measured with the well counter at the end of the SPECT scan.
2. The arterial input function for the compartment model studies was defined from the plasma radioactivity concentration curve, rather than the whole blood radioactivity curve. K_1 is therefore the regional "plasma" flow. Thus, for comparison with the microsphere flow measurements, which estimates the whole blood flow, K_1 was divided by (1−Hct) to obtain the flow for the total blood.
3. For a tracer with limited first-pass EF<1.0, flow (MBF) is related to K_1 by K_1=EF×MBF. The first-pass EF is flow-dependent and decreases at high flow. We have applied an empirical formulation for the first-pass EF based on the data by Weich et al. [10] ($EF=0.84-0.524\cdot\log_{10}(K_1^*)$ where K_1^* is $K_1/(1-\mathrm{Hct})$. The K_1 values obtained with two- and three-compartment models with/without corrections according to Eq. 1 were compared to the average of microsphere blood flow values obtained pre- and post-dynamic SPECT scan.

The distribution volume of ^{201}Tl (V_d) was defined as

$$V_d = \frac{K_1}{k_2} \text{ for the two} - \text{compartment model} \quad (2a)$$

$$V_d = \frac{K_1}{K_2}\left(1+\frac{K_3}{K_4}\right) \text{ for the three} - \text{compartment model.} \quad (2b)$$

As mentioned before, the resting studies were collected for 4 h, whilst the adenosine and beta-blocker studies were collected for approximately 1 h. To investigate whether the shorter collection time introduces systematic bias, NLLSF fits restricted to the first 1 h of the resting study data were also performed and compared with the V_d values from the full 4 h resting data set and with the estimates obtained from the beta-blocker and adenosine studies.

Akaike information criterion (AIC) and Schwarz criterion (SC) were calculated for both two-compartment and three-compartment model fits [16] to test the adequacy of the two models. All data are presented as mean±1 SD. Student's t test was employed in the comparison of the V_d values. Pearson's regression analysis was applied to compare K_1 and microsphere flow values. A probability value of <0.05 was considered statistically significant.

Results

Figure 3 shows the plasma to whole blood concentration ratios in the six dogs with rapid plasma separation and the averaged data. Equilibrium is reached after about 40 min, at which time the mean ratio was found to be 0.76. As expected, relative plasma concentration is highest early on as the tracer is injected into the plasma (and not red blood cells). ^{201}Tl is rapidly cleared from the plasma causing a rapid decline in relative plasma concentration and "undershoot" before equilibrium is established. Samples left for a prolonged period before plasma separation showed the value of approximately 0.78, which was close to the plasma to whole blood concentrations ratio at the equilibrium shown in

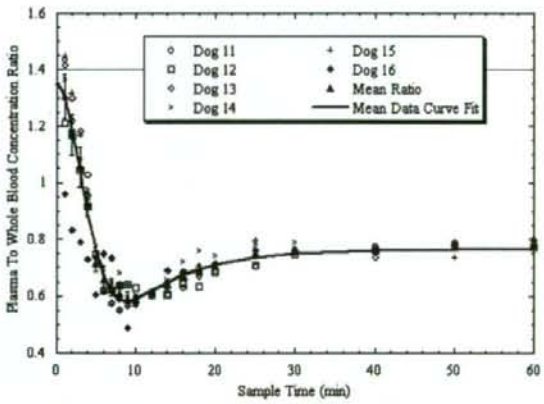

Fig. 3 Individual and mean plasma to whole blood concentration ratios over time for the six dogs with rapid plasma separation. *Error bars* indicate the standard error of the mean. *Solid line* is the curve fit to mean ratio data

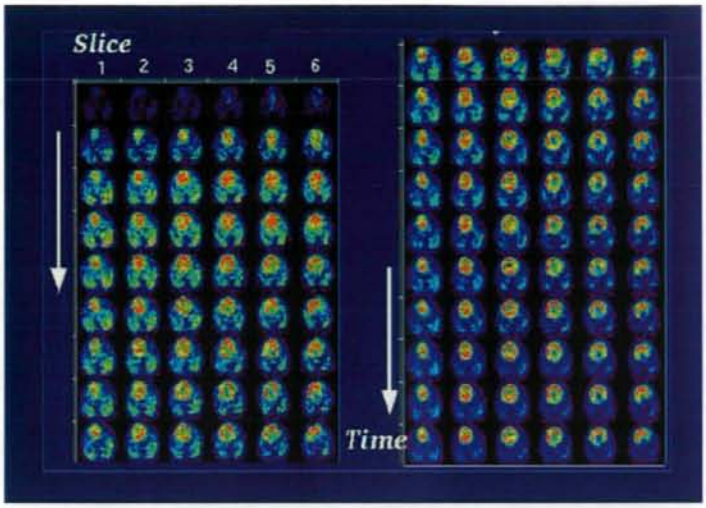

Fig. 4 A typical example of sequential SPECT images of the myocardium for six representative slices after intravenous injection of ^{201}Tl into a canine at rest

Fig. 3. The plasma to whole blood ratio curves could be approximated by the following equation:

$$R_{\mathrm{pl/wb}} = A_0 e^{-\lambda(t+\Delta t)^2} + A_1\left(1 - e^{-\lambda_2(t+\Delta t)}\right), \qquad (3)$$

which resulted in A_0=1.303±0.045, A_1=0.7649±0.0056, λ_1=0.03636±0.0039 min^{-1}, λ_2=0.1263±0.0077 min^{-1} and Δt=0.9516±0.41 min. The correlation coefficient for the fit was r=0.995.

Figure 4 shows a typical example of sequential images after the intravenous injection of ^{201}Tl for six representative slices of a dog studied at rest. It can be seen that ^{201}Tl appeared in the ventricular chambers first and then gradually accumulated homogeneously into the left myocardium. The quality of these images is reasonably good, indicating that our approach of estimating the kinetic parameters by NLLSF is feasible without excessive noise

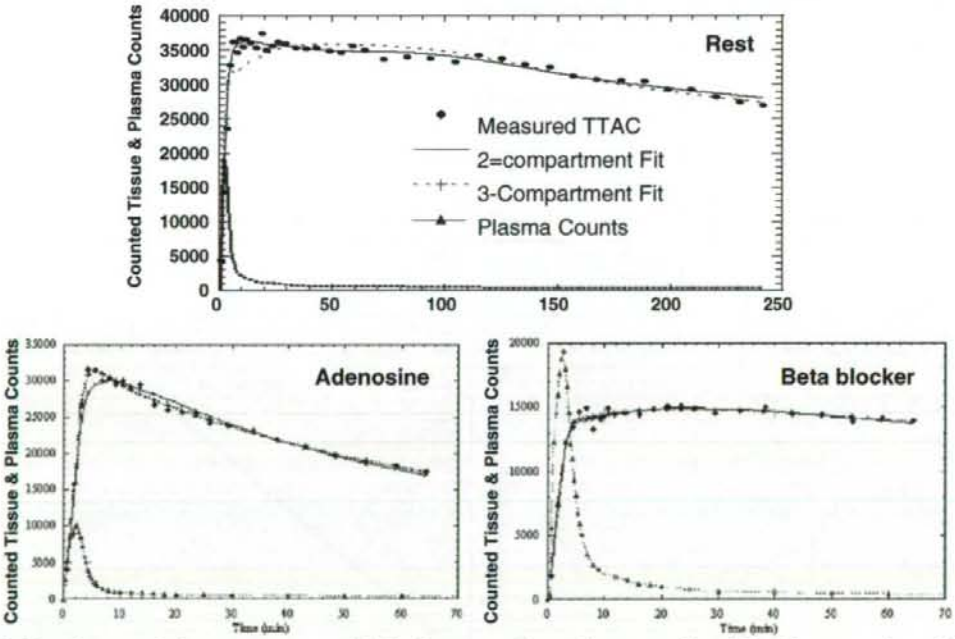

Fig. 5 TTACs and two- and three-compartment model fits for a resting, adenosine (increased MBF) and beta-blocker (reduced MBF) study. Note the different time scales for the resting study because resting studies were collected for 4 h compared to ≈1 h for the pharmacological intervention studies

amplification. Curve fits to representative TTACs for resting, beta-blocker and adenosine infusion studies are shown in Fig. 5. The height of the TTACs relative to the input function corresponded well with the pharmacological challenges. Compared to the resting studies, peaks of TTACs relative to the arterial input function were higher for adenosine and lower after beta-blocker administration. Results of kinetic fitting by the two- and three-compartment models are also plotted on this figure. Visually, the three-compartment model provided better fits than the two-compartment model to the observed TTACs, which is particularly evident for the initial scan period of the resting and adenosine studies.

Shown in Fig. 6a–e is the comparisons of K_1 obtained by NLLSF (three-compartment model fit) with the microsphere flow estimates. Values were averaged over the myocardial segments in both axes, thus each point corresponds to a single study. There was good correlation between K_1 and the microsphere flow when no corrections were applied, but K_1 significantly under-estimated the true flow (Fig. 6a). All the corrections improved the K_1 estimates (Fig. 6b–d) and the best agreement between K_1 and microsphere flow was observed when all three factors were corrected as described in Eq. 1 (Fig. 6e). Results of the regression analysis also demonstrated the highest correlation coefficient when all three correction factors were applied. Table 1 summarises the results of the Akaike information criteria (AIC) and Schwartz criteria (SC) obtained from the kinetic fitting analysis for all myocardial segments of all subjects. Both

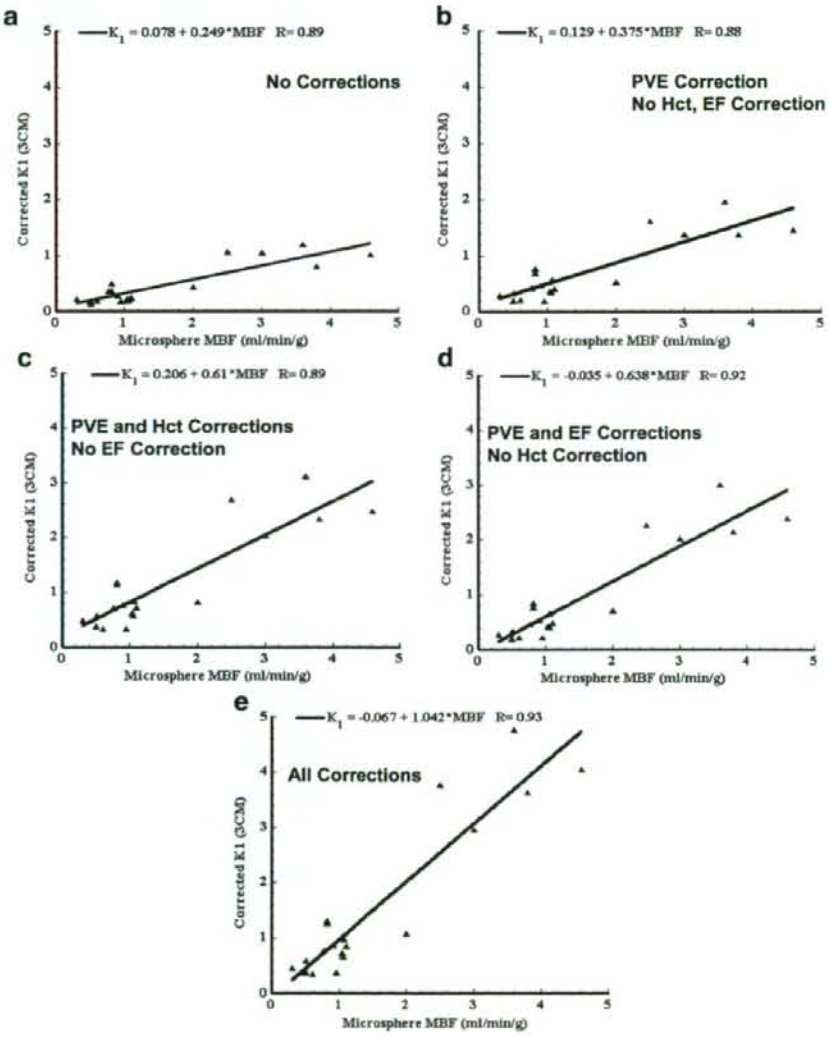

Fig. 6 Plot of K_1 derived from the three-compartment model fit against the mean of the pre- and post-dynamic SPECT microsphere blood flow measurements. **a** No correction for PVE, limited first-pass EF or conversion from plasma to blood flow has been applied. **b** Correction for PVE has been applied, but not for Hct or limited first-pass EF. **c** Corrections for PVE and Hct have been applied, but not for limited first-pass EF. **d** Corrections for PVE and limited first-pass EF have been applied, but not for Hct. **e** All corrections are applied for PVE, limited first-pass EF and Hct

Table 1 Summary of improvement in fit with the three-compartment model over the two-compartment model

Study group	Number of curves	Mean AIC two-compartment	Mean AIC three-compartment	Mean SC two-compartment	Mean SC three-compartment	Number of curves (%) (three-compartment better than two-compartment)[a]
Resting	35	652.4	630.2 ($p<0.01$)	663.8	638.4 ($p<0.01$)	24 (69)
Beta-blocker	20	378.4	378.8 (p=n.s.)	382.0 ($p<0.01$)	384.7	3 (15)
Adenosine	45	405.1	393.6 ($p<0.01$)	408.7	399.5 ($p<0.01$)	28 (62)

The p value indicates that the value in the cell is significantly lower than the corresponding other value.
AIC: Akaike information criterion, *SC*: Schwarz criterion
[a]This column gives the number of TTAC fits where the three-compartment model fit provided a significant improvement over the two-compartment fit according to all criteria (AIC, SC).

AIC and SC demonstrated that the three-compartment model fit provided significant improvement over the two-compartment model fit for resting and adenosine studies. For the beta-blocker studies, AIC between the two model fits was not significantly different, whilst SC demonstrated significantly better fit with the two-compartment model. Improved AIC and SC for the three-compartment model fit were observed in 69% of resting TTACs and 62% of adenosine TTACs, but only 15% in beta-blocker TTACs.

As shown in Fig. 7a and b, the K_1 and V_d values derived from the two-compartment model fit showed significant differences compared with those by the three-compartment model. Both K_1 and V_d were under-estimated with the two-compartment model fit compared with the three-compartment model fit. It should, however, be noted that there was a good correlation between the two- and three-compartment models for K_1, thus the bias introduced by the two-compartment model fit can potentially be corrected. K_1 values by the three-compartment model fit with all three corrections were 0.86±0.36, 2.71±1.64 and 0.55±0.24 ml/min/g corresponding to rest, adenosine infusion (with constant infusion at 140–700 mg/kg/h) and beta-blocker (with 2–6 mg administration), respectively. Difference in V_d was less than 10% and again this bias can potentially be corrected by the regression equation. The K_1 obtained with the two-compartment model also demonstrated a good correlation with the microsphere flow (Fig. 7c), though there was again a systematic under-estimation in K_1.

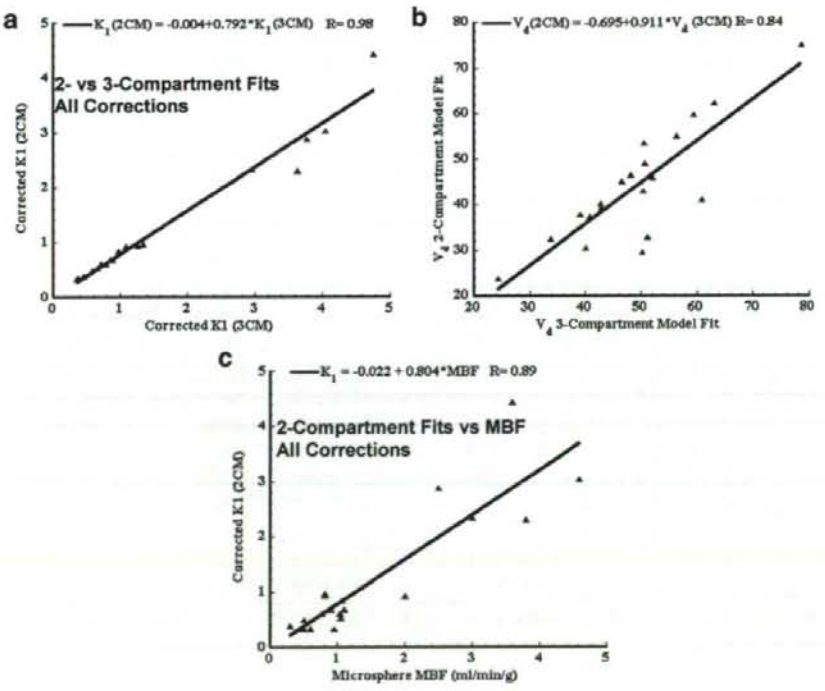

Fig. 7 **a** Plot of K_1 estimates derived from the two-compartment model fit against those from the three-compartment model fit. **b** Plot of V_d estimates derived from the two-compartment model fit against those from the three-compartment model fit. **c** Plot of K_1 values derived from the two-compartment model fit against mean of the pre- and post-dynamic SPECT microsphere blood flow measurements

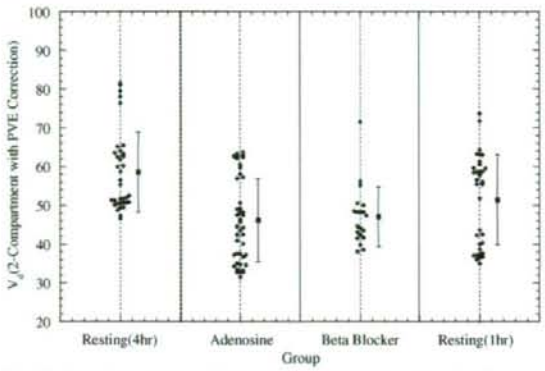

Fig. 8 V_d values obtained from the two-compartment model fit to the full 4 h resting data, adenosine and beta-blocker infusion 1 h curves and fit to first 1 h only of the resting study curves. Data from the multiple individual myocardial regions are shown

Figure 8 plots the V_d values for all evaluated myocardial segments for the fit to 4 h resting data, adenosine and beta-blocker infusion 1 h data and fit to only the first 1 h of resting data. The 4-h resting V_d values are significantly higher ($p<0.01$) compared with the adenosine, beta-blocker values and compared with the fit to the first 1 h resting data. However, the 1-h resting values are not significantly different from the beta-blocker V_d values nor the adenosine values.

Discussion

This study demonstrates that the kinetic analysis of quantitatively assessed myocardial ^{201}Tl accumulation (build-up and washout in healthy canines) provided quantitative MBF values, which agreed well with flows obtained using microspheres for a wide physiological range of flows. The size of the TTACs relative to the arterial plasma concentration corresponded well to the pharmacological stresses induced by adenosine and beta-blocker challenges. The compartmental model approach could reproduce these TTACs to make the determination of kinetic parameters, such as K_1 and V_d, possible. The three-compartment model gave results which were generally higher than the two-compartment model and which were statistically significantly better in terms of AIC, SC for the resting and adenosine studies, and this was in line with the visual inspection of the TTAC model fit curves. It should, however, be noted that the differences were only small between the two- and three-compartment model approaches, approximately 20% for K_1 and 10% for V_d The bias associated with the two-compartment model could be corrected by a linear regression as shown in Fig. 7a–c. This opens the possibility of using the more reliable two-compartment model fit due to its reduced number of parameters for routine clinical studies. The improved reliability of the two-compartment model fit in the clinical setting is particularly important if one intends to shorten the study time or generate parametric images.

The three corrections for PVE, Hct and first-pass EF proved to be important. The PVE correction method used in this work cannot, however, be applied to clinical studies, and the PVE correction in the beating heart still remains a considerable challenge in clinical studies. PVE may be reduced by gating the data, which may not, however, be feasible for the already noisy and large dynamic SPECT data sets. PVE may also be reduced by including resolution recovery as part of the reconstruction process [17–20]. Alternatively, it may also be possible to include PVE as part of the kinetic model fitting [21–25]. However, this adds extra fitting parameters and requires some parameters to be assumed fixed.

The input function is an important component in compartment model fitting. In this study, rapid arterial blood sampling was performed, and the plasma was separated by centrifugation. A number of important insights were gained by performing rapid separation of plasma in a subset of samples and dogs. It was found that ^{201}Tl enters the red blood cells as observed from the rapid separation of plasma in a subset of samples and dogs, which is not un-expected as potassium is also known [22] to be taken up by the red blood cells. The exchange of ^{201}Tl between red blood cells and plasma is relatively slow compared to the passage of blood through the capillary bed and hence direct uptake of activity from the red blood cells into tissue is believed to be negligible. Hence, tissue uptake will be dominated by the activity in the plasma during passage through the capillary bed and plasma in the substrate being measured. As a consequence, the flow measurement obtained with ^{201}Tl is plasma flow, which is in contrast to the microsphere studies, which measure whole blood flow. Conversion of plasma to blood flow was achieved by dividing the plasma flow by (1−Hct), as shown in Eq. 1, which then allowed the direct comparison with the microsphere measurements.

Rigorous estimation of the input function requires frequent arterial blood sampling. This is not only considered invasive, but also labor intensive. In addition, it has been shown in this study that rapid separation of the plasma for at least the first 30–40 min post-^{201}Tl administration is required to obtain accurate plasma concentration. If the separation of plasma is delayed, then the true plasma concentration at the time of sampling cannot be measured, which results in biased K_1 estimates. An empirical relationship of plasma to whole blood ratio as a function of time was developed and was found to be sufficiently consistent between dogs (Fig. 3) to allow the mean curve to be applied with minimal bias. Thus, in clinical practice, whole blood samples may be counted and converted to plasma concentration using the empirical relationship. This also potentially allows the input function to be obtained

non-invasively from the SPECT data using, for example, a curve derived from a left ventricular region. However, it should be noted that the relationship between plasma and whole blood counts in this study was derived for a 4-min infusion protocol and may be different for other injection protocols, such as bolus injection. Previously, it has been shown that population-based input functions calibrated with one or two blood samples could avoid the need for frequent arterial blood samples [26–28]. There is also a potential for applying this approach to ^{201}Tl studies. This is beyond the scope of this study and a systematic study should be designed to confirm this in clinical settings.

^{201}Tl has a high trans-capillary EF and thus the initial regional uptake of this tracer predominantly reflects the regional blood flow [10]. Use of a tracer that has a high first-pass EF is essential when one intends to quantitatively assess MBF at a high flow range or the coronary flow reserve. The EF of ^{201}Tl is reported as >0.8 [10] for a wide flow range and is known to be higher than ^{99m}Tc-labelled tracers such as tetrofosmine and sestamibi [29]. The physical characteristics of ^{201}Tl are unfortunately not ideal as low energy emission increases the attenuation factor and the scatter in the image. In addition, the relatively long half-life limits the administered activity to about a tenth of that with ^{99m}Tc tracers. Despite these shortcomings, the physiological characteristics of having high first-pass EF make ^{201}Tl an interesting tracer particularly for the absolute quantitation of MBF and the coronary flow reserve. This study demonstrates that quantitative physiological parameters can be derived from dynamic ^{201}Tl SPECT studies, despite its less than ideal imaging characteristics.

Whilst the quantitative physiological parameter estimation removed the systematic bias between MBF estimated by ^{201}Tl dynamic SPECT and by microspheres, the spread of data points around the regression line was rather large (Figs. 6e and 7c). This is not only due to possible errors in the estimation of MBF from the ^{201}Tl, but there was also considerable variation in flow estimated by the microspheres at the beginning and end of the study. Thus, at least part of the variability is attributable to errors in microsphere flow measurement, and particularly for the pharmaceutical intervention studies, flow may not have remained constant throughout the entire study duration, which may also account for some of the differences seen between the various flow measurements.

V_d estimated in this study could serve as an index of viability, as viable myocytes are required to maintain the large concentration gradient between plasma and myocardium at equilibrium. There was no significant difference in V_d values between rest, beta-blocker and adenosine studies when fitted for 1 h (Fig. 8). The significant difference between the 1- and 4-h fit for resting data could be explained by the limitation of the two-compartment model. Considerable spread in the V_d values observed over all dog studies on the other hand was partially attributed to the short (insufficient) scan time for reliable estimates of V_d. With the exception of the large, outlying V_d values in all 5 regions of 1 dog, the resting V_d values fell within a relatively narrow range of 47 to 65 (mean±SD=55±6). Given the sufficiently long scan time, significant reduction in V_d in infarcted areas may be detected. However, this would need to be tested with a suitable study design.

The scan time of 4 h required to achieve reliable V_d estimates is not practical in the routine clinical setting. As has been shown by Lau et al. [30], the scan period may be split into two sessions, an early dynamic scan for 30 min followed by a single static scan at approximately 3 h. This scheme is not more onerous than current rest/re-distribution protocols and hence could be practical. In addition, it may be possible to simplify the scanning protocol further to two static scans by using the table look-up method for the two-compartment model, which has been successfully employed for other SPECT tracers with relatively slow kinetics similar to ^{201}Tl [27, 31, 32]. This warrants further investigation.

This study relies on established, rigorous attenuation and scatter correction in SPECT [5] and availability of multi-detector SPECT systems capable of performing dynamic acquisition. To our knowledge, this is the first report that has demonstrated that it is possible to obtain quantitative physiological parameter estimates of K_1 and V_d in the myocardium using a clinical SPECT scanner and ^{201}Tl. This work suggests that it is feasible to apply our technique to clinical studies. Further studies are, however, needed to validate the proposed approach in the clinical setting. Incomplete motion correction is one possible error source, particularly in patients. Dynamic SPECT is probably more sensitive to the possible movement of patients during the study. Shortened clinical protocol is preferred, but this requires additional development to improve the reliability of parameter estimates. In addition, two scanning sessions are needed to assess the coronary flow reserve. We have recently demonstrated a technique to assess two cerebral blood flow images, one at rest and another after a vasodilating drug, from a single session of a SPECT scan in conjunction with split dose administration of ^{123}I-iodoamphetamine and dynamic SPECT [7]. As a clinical implication, the quantitative assessment of MBF and coronary flow reserve is important. For instance, coronary micro-vascular dysfunction or impaired endothelial function in patients with coronary risk factors or patients with cardiomyopathy or with heart failure is an un-resolved important issue to answer [11]. Coronary flow reserve can be reduced in patients with hypercholesterolemia without overt coronary stenosis [12]. A systematic study should be carried out to validate this approach for assessing MBF at rest and after adenosine from a single session of a scan.

Acknowledgement This study was supported by the Budget for Nuclear Research of the Ministry of Education, Culture, Sports, and Technology (MEXT), Japan; a grant from the Cooperative Link of Unique Science and Technology for Economy Revitalization promoted by the Ministry of Education, Culture, Sports and Technology, Japan and a grant for translational research from the Ministry of Health, Labour and Welfare (MHLW), Japan. We would like to thank Nihon Medi-Physics, Hyogo, Japan for providing the ^{201}Tl samples and also Mr. Yoshihide Takatani for his invaluable suggestion on the study design.

References

1. Gullberg GT, Huesman RH, Ross SG, et al. Dynamic cardiac single-photon emission computed tomography. In: Beller GA, Zaret BL, editors. Nuclear cardiology: state of the art and future directions. Philadelphia, PA: Mosby-Year Book Inc.; 1998. p. 137–87.
2. Chiao PC, Ficaro EP, Dayanikli F, Rogers WL, Schwaiger M. Compartmental analysis of technetium-99m-teboroxime kinetics employing fast dynamic SPECT at rest and stress. J Nucl Med 1994;35(8):1265–73.
3. Narita Y, Eberl S, Iida H, Hutton BF, Braun M, Nakamura T, et al. Monte Carlo and experimental evaluation of accuracy and noise properties of two scatter correction methods for SPECT. Phys Med Biol 1996;41(11):2481–96.
4. Narita Y, Iida H, Eberl S, Nakamura T. Monte Carlo evaluation of accuracy and noise properties of two scatter correction methods for ^{201}Tl cardiac SPECT. IEEE Trans Nucl Sci 1997;44:2465–72.
5. Iida H, Shoji Y, Sugawara S, Kinoshita T, Tamura Y, Narita Y, et al. Design and experimental validation of a quantitative myocardial ^{201}Tl SPECT System. IEEE Trans Nucl Sci 1999;46:720–6.
6. Iida H, Narita Y, Kado H, Kashikura A, Sugawara S, Shoji Y, et al. Effects of scatter and attenuation correction on quantitative assessment of regional cerebral blood flow with SPECT. J Nucl Med 1998;39(1):181–9.
7. Kim KM, Watabe H, Hayashi T, Hayashida K, Katafuchi T, Enomoto N, et al. Quantitative mapping of basal and vasareactive cerebral blood flow using split-dose ^{123}I-iodoamphetamine and single photon emission computed tomography. Neuroimage 2006;33(4):1126–35.
8. Beller GA, Watson DD, Pohost GM. Kinetics of thallium distribution and redistribution: clinical applications in sequential myocardial imaging. In: Pitt B, Strauss HW, editors. Cardiovascular nuclear medicine. St. Louis: Mosby; 1979. p 225–42.
9. Berman DS, Maddhi J, Garcia EV. Role of thallium-201 imaging in the diagnosis of myocardial ischemia and infarction. In: F HS, editor. Nuclear medicine annual. New York: Raven; 1980. p 1–55.
10. Weich HF, Strauss HW, Pitt B. The extraction of thallium-201 by the myocardium. Circulation 1977;56(2):188–91.
11. Camici PG, Crea F. Coronary microvascular dysfunction. N Engl J Med 2007;356(8):830–40.
12. Yokoyama I, Ohtake T, Momomura S, Nishikawa J, Sasaki Y, Omata M. Reduced coronary flow reserve in hypercholesterolemic patients without overt coronary stenosis. Circulation 1996;94 (12):3232–8.
13. Li J, Tsuji BMW, Welch A, Frey EC, Gullberg GT. Energy window optimization in simultaneous Technetium-99m and Thallium-201 SPECT data acquisition. IEEE Trans Nucl Sci 1995;42:1207–13.
14. Meikle SR, Hutton BF, Bailey DL. A transmission-dependent method for scatter correction in SPECT. J Nucl Med 1994;35(2):360–7.
15. Hudson HM, Larkin RS. Accelerated image reconstruction using srdered subsets of projection data. IEEE Trans Med Imag 1994;13:601–9.
16. Choi Y, Hawkins RA, Huang SC, Brunken RC, Hoh CK, Messa C, et al. Evaluation of the effect of glucose ingestion and kinetic model configurations of FDG in the normal liver. J Nucl Med 1994;35(5):818–23.
17. Hutton BF, Hudson HM, Beekman FJ. A clinical perspective of accelerated statistical reconstruction. Eur J Nucl Med 1997;24 (7):797–808.
18. Hutton BF, Lau YH. Application of distance-dependent resolution compensation and post-reconstruction filtering for myocardial SPECT. Phys Med Biol 1998;43(6):1679–93.
19. Pretorius PH, King MA, Pan TS, de Vries DJ, Glick SJ, Byrne CL. Reducing the influence of the partial volume effect on SPECT activity quantitation with 3D modelling of spatial resolution in iterative reconstruction. Phys Med Biol 1998;43(2): 407–20.
20. Soares EJ, Glick SJ, King MA. Noise chaeacterization of combined Bellini-type attenuation correction and frequency-distance principle restoration filtering SPECT. IEEE Trans Nucl Sci 1996;43:3278–90.
21. Iida H, Kanno I, Takahashi A, Miura S, Murakami M, Takahashi K, et al. Measurement of absolute myocardial blood flow with H215O and dynamic positron-emission tomography. Strategy for quantification in relation to the partial-volume effect. Circulation 1988;78(1):104–15.
22. Araujo LI, Lammertsma AA, Rhodes CG, McFalls EO, Iida H, Rechavia E, et al. Noninvasive quantification of regional myocardial blood flow in coronary artery disease with oxygen-15-labeled carbon dioxide inhalation and positron emission tomography. Circulation 1991;83(3):875–85.
23. Bergmann SR, Herrero P, Markham J, Weinheimer CJ, Walsh MN. Noninvasive quantitation of myocardial blood flow in human subjects with oxygen-15-labeled water and positron emission tomography. J Am Coll Cardiol 1989;14(3):639–52.
24. Iida H, Rhodes CG, de Silva R, Yamamoto Y, Araujo LI, Maseri A, et al. Myocardial tissue fraction-correction for partial volume effects and measure of tissue viability. J Nucl Med 1991;32(11): 2169–75.
25. Iida H, Tamura Y, Kitamura K, Bloomfield PM, Eberl S, Ono Y. Histochemical correlates of (15)O-water-perfusable tissue fraction in experimental canine studies of old myocardial infarction. J Nucl Med 2000;41(10):1737–45.
26. Iida H, Itoh H, Nakazawa M, Hatazawa J, Nishimura H, Onishi Y, et al. Quantitative mapping of regional cerebral blood flow using iodine-123-IMP and SPECT. J Nucl Med 1994;35(12):2019–30.
27. Onishi Y, Yonekura Y, Nishizawa S, Tanaka F, Okazawa H, Ishizu K, et al. Noninvasive quantification of iodine-123-iomazenil SPECT. J Nucl Med 1996;37(2):374–8.
28. Takikawa S, Dhawan V, Spetsieris P, Robeson W, Chaly T, Dahl R, et al. Noninvasive quantitative fluorodeoxyglucose PET studies with an estimated input function derived from a population-based arterial blood curve. Radiology 1993;188(1):131–6.
29. Fukushima K, Momose M, Kondo C, Kusakabe K, Kasanuki H. Myocardial kinetics of (201)Thallium, (99m)Tc-tetrofosmin, and (99m)Tc-sestamibi in an acute ischemia–reperfusion model using isolated rat heart. Ann Nucl Med 2007;21(5):267–73.
30. Lau CH, Eberl S, Feng D, Iida H, Lun PK, Siu WC, et al. Optimized acquisition time and image sampling for dynamic SPECT of Tl-201. IEEE Trans Med Imag 1998;17(3): 334–43.
31. Iida H, Itoh H, Bloomfield PM, Munaka M, Higano S, Murakami M, et al. A method to quantitate cerebral blood flow using a rotating gamma camera and iodine-123 iodoamphetamine with one blood sampling. Eur J Nucl Med 1994;21(10):1072–84.
32. Onishi Y, Yonekura Y, Mukai T, Nishizawa S, Tanaka F, Okazawa H, et al. Simple quantification of benzodiazepine receptor binding and ligand transport using iodine-123-iomazenil and two SPECT scans. J Nucl Med 1995;36(7):1201–10.

Eur J Nucl Med Mol Imaging (2008) 35:1899–1911
DOI 10.1007/s00259-008-0796-z

ORIGINAL ARTICLE

Non-invasive estimation of hepatic blood perfusion from $H_2{}^{15}O$ PET images using tissue-derived arterial and portal input functions

N. Kudomi · L. Slimani · M. J. Järvisalo · J. Kiss · R. Lautamäki · G. A. Naum · T. Savunen · J. Knuuti · H. Iida · P. Nuutila · P. Iozzo

Received: 30 August 2007 / Accepted: 25 March 2008 / Published online: 6 May 2008

Abstract
Purpose The liver is perfused through the portal vein and the hepatic artery. When its perfusion is assessed using positron emission tomography (PET) and ^{15}O-labeled water ($H_2{}^{15}O$), calculations require a dual blood input function (DIF), i.e., arterial and portal blood activity curves. The former can be generally obtained invasively, but blood withdrawal from the portal vein is not feasible in humans. The aim of the present study was to develop a new technique to estimate quantitative liver perfusion from $H_2{}^{15}O$ PET images with a completely non-invasive approach.

Methods We studied normal pigs (n=14) in which arterial and portal blood tracer concentrations and Doppler ultrasonography flow rates were determined invasively to serve as reference measurements. Our technique consisted of using model DIF to create tissue model function and the latter method to simultaneously fit multiple liver time–activity curves from images. The parameters obtained reproduced the DIF. Simulation studies were performed to examine the magnitude of potential biases in the flow values and to optimize the extraction of multiple tissue curves from the image.
Results The simulation showed that the error associated with assumed parameters was <10%, and the optimal number of tissue curves was between 10 and 20. The estimated DIFs were well reproduced against the measured ones. In addition, the calculated liver perfusion values were not different between the methods and showed a tight correlation (r=0.90).
Conclusion In conclusion, our results demonstrate that DIF can be estimated directly from tissue curves obtained through $H_2{}^{15}O$ PET imaging. This suggests the possibility to enable completely non-invasive technique to assess liver perfusion in patho-physiological studies.

Keywords Hepatic blood flow · Input function · Portal vein · Positron emission tomography · $H_2{}^{15}O$

N. Kudomi (✉) · L. Slimani · M. J. Järvisalo · R. Lautamäki · G. A. Naum · J. Knuuti · P. Nuutila · P. Iozzo
Turku PET Centre, University of Turku,
P.O. Box 52, 20521 Turku, Finland
e-mail: nobuyuki.kudomi@tyks.fi

J. Kiss · T. Savunen
Department on Surgery, University of Turku,
Turku, Finland

H. Iida
Department of Investigative Radiology,
Advanced Medical-Engineering Center,
National Cardiovascular Center-Research Institute,
5-7-1, Fujishirodai,
Suita, Osaka 565-8565, Japan

P. Nuutila
Department of Medicine, University of Turku,
Turku, Finland

P. Iozzo
Institute of Clinical Physiology, National Research Council,
56100 Pisa, Italy

Introduction

The quantitative determination of hepatic blood flow has the potential to provide important information in the assessment and follow-up of liver disorders, which are almost invariably accompanied by abnormalities in organ

perfusion, representing a prognostic indicator and responding to disease amelioration [4, 10, 19, 21, 28–31, 35]. Positron emission tomography (PET) and ^{15}O-labeled water ($H_2{}^{15}O$) enable to assess hepatic perfusion quantitatively [29, 30, 35], as based on tracer kinetic modeling, requiring the notion of the time variation of radiotracer concentrations in the liver tissue and in the blood entering the organ (input function).

The liver is characterized by a dual blood supply, comprising the hepatic artery and the portal vein, draining venous blood from the gastrointestinal tract. Thus, in the modeling of PET data from liver, two blood time–activity curves are required to represent the input function (dual input function [DIF]). However, blood withdrawal from a peripheral artery [8, 9, 16, 17, 26, 33] is not always successful and risk-free, and it requires careful correction in time delay between the sampling site and the tissue. More importantly, the portal vein cannot be accessed from any peripheral site, making its blood collection impractical in humans.

The aim of the present study was to develop a new technique to estimate the two components of the DIF non-invasively from dynamic $H_2{}^{15}O$ PET images. The present method was characterized by use of a model input function to create a tissue model function, which was used to simultaneously fit multiple tissue curves from PET image. The parameter obtained in the input function model reproduced the input function. Computer simulation studies were performed to examine the magnitude of potential biases in the parameter estimates caused by the inherent assumptions and to optimize the extraction of multiple tissue curves from the image. The present investigation was conducted in pigs because the comparison between measured and estimated values necessitated deep catheterization and invasive Doppler flow measurements.

Materials and methods

Theory and computation of non-invasive DIF

A model function was created to shape the input function according to the dose of tracer, administration process, body weight, and physiological state in each subject [18]. The model function introduced is

$$\begin{aligned} C_A(t) &= 0. && (t < t_1) \\ &= \frac{A}{K_e^2(1+\alpha)^2}\left(1 - \exp\left(K_e(1+\alpha)(t_1 - t)\right)\right) && (t_1 \le t \le t_2) \\ &= \frac{A}{K_e^2(1+\alpha)^2}\left(\exp\left(K_e(1+\alpha)(t_1 - t_2)\right) + \exp\left(K_e(1+\alpha)(t_2 - t)\right) - 2\cdot\exp\left(K_e(1+\alpha)(t_1 - t)\right)\right) && (t > t_2) \end{aligned} \quad (1)$$

Details of the model function are given in the Appendix. Briefly, A indicates the height, and t_1 and t_2-t_1 indicate the appearance time of tracer and administration duration, respectively. K_e (ml/min) and $K_i(=\alpha K_e)$ (ml/min) represent the tracer bidirectional diffusion rates between arterial blood and whole body interstitial spaces, respectively.

The portal vein blood model function was generated by introducing the gut compartment model [29–31, 35], that is, a single compartment model between arterial blood and gut compartment, assuming no difference in appearance time between arterial and portal blood (or delay time of portal input), with diffusion rate k_g in the gut system as

$$C_P(t) = k_g C_A(t) \otimes e^{-k_g \cdot t} \quad (2)$$

Using these arterial and portal input model functions, the tissue response function can be expressed by assuming a single tissue compartment model [29–30, 35] and that tracers in arterial and portal blood were well mixed before exchange with liver tissue as

$$C_{TIS}(t) = \left(f_a C_A(t) + f_p C_P(t)\right) \otimes e^{-k_2 \cdot t} \quad (3)$$

where k_2 is defined as $(f_a+f_p)/V_L$, and V_L (ml/g) is the distribution volume of water between blood and tissue. In the present study, V_L was fixed to 0.7 ml/g, which was suggested to fix in a sensitivity analysis by Ziegler et al. [35] and was obtained as 0.71±0.03 ml/g for same subjects in our preliminary evaluation using measured blood input functions. Including a blood volume term into this equation, the model function for liver tracer concentrations, as measured by PET (C_{PET}), can be expressed as

$$C_{PET}(t) = (1 - V_0)\left(f_a C_A(t) + f_p C_P(t)\right) \otimes e^{-k_2 \cdot t} + V_0 C_{input}(t) \quad (4)$$

where $C_{input}(t)$ is defined as

$$C_{input}(t) = r_a C_A(t) + r_p C_P(t) \quad (5)$$

where r_a and r_p are arterial (f_a ml/min/g) and portal vein blood flow (f_p ml/min/g) ratios to total hepatic flow, i.e., $r_a=f_a/(f_a+f_p)$ and $r_p=f_p/(f_a+f_p)$ [35]. The flow chart to estimate input functions in this procedure is simplified in

Fig. 1. Multiple tissue time–activity curves (TAC) from liver image were used to estimate the input functions. First, the model function in Eq. 4 was individually fitted to tissue TACs, assuming that k_g in Eq. 2 is constant by a non-linear fitting method (variable-metric method in the PAW environment: version 2.13/08 [http://wwwasd.web.cern.ch/wwwasd/paw/]), and the set of seven parameters of A, t_1, t_2, $K_e(1+\alpha)$, f_a, f_p, and V_0 in Eqs. 1 and 4 was obtained for each tissue TAC. Then, means and standard deviations of t_1, t_2, and $r_a(=f_a/(f_a+f_p))$ were calculated, and the tissue TACs with values of t_1 or $t_2>1$ standard deviation of respective means were excluded to avoid the potential influence of TACs outside the liver. In the second step, assuming that all parts of the liver share the same input functions, values of t_1, t_2, and r_a were fixed to their means, and the other two parameters (A and $K_e(1+\alpha)$) were estimated by minimizing the following equation:

$$S^2 = \sum_{i\in Tis}\sum_{k}\left(C_{PET}^{i,k} - \left((1-V_0^i)\left(f_a^i C_A(t) + f_p^i C_P(t)\right) \otimes e^{-k_2^i t} + V_0^i C_{input}(t)\right)\right)^2 \quad (6)$$

where $C_{PET}^{i,k}$ is the tissue TAC for kth frame in ith tissue region of interest, t is the corresponding time of kth frame, and f_a^i, $f_p^i(=f_a^i(1-r_a)/r_a)$ and V_0^i are values of arterial and portal vein blood flows and of blood volume for ith tissue, respectively. In this procedure, S^2 was minimized by the grid search method *to* avoid dependency of initial guess, where S^2 was calculated for 1,000 discrete values of both A and $K_e(1+\alpha)$ between ranges of three standard deviations from respective mean values, omitting the negative value. In this procedure, for a given input function, i.e., given A and $K_e(1+\alpha)$, f_a and V_0 for each TAC were computed by the grid search method, with acceptable ranges of 0–100 ml/min/g and 0–1 ml/ml, and steps of 1 ml/min/g and 0.01 ml/ml, respectively, and then substituted in Eq. 6. Finally, the image-based input function was obtained by substituting the estimated parameters into Eq. 1.

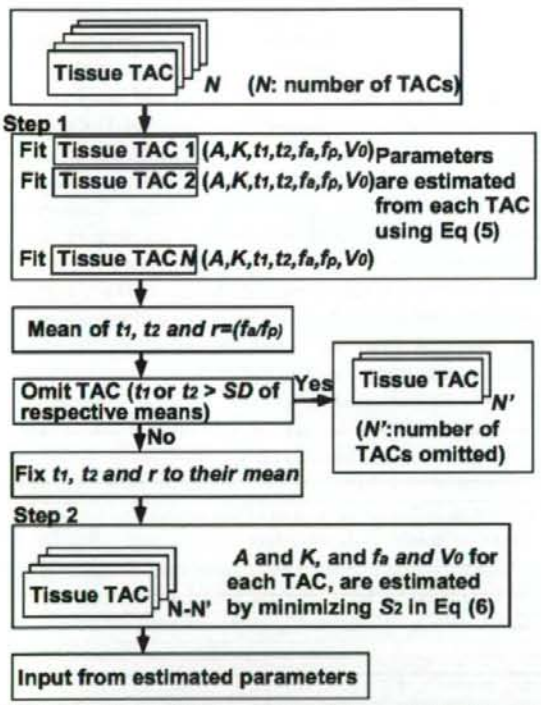

Fig. 1 A schematic diagram of the procedure to estimate the input functions using multiple tissue TACs. *Step 1* The model function (Eq. 4) was individually fitted to N tissue time–activity curves (*TAC*). Then, means and standard deviations of t_1, t_2, and r_a were calculated, and the tissue TACs with values of t_1 or $t_2>1$ standard deviation of respective means were excluded (indicated as N' TACs) to avoid the potential influence of TACs outside the liver. In the second step, assuming that all parts of the liver share the same input functions, values of t_1, t_2, and r_a were fixed to their means, and the other two parameters (A and $K_e(1+\alpha)$) were estimated by minimizing Eq. 6 by the grid search method. Finally, the image-based input function was obtained by substituting the estimated parameters into Eq. 1

Simulation study

The present method for generating portal vein input assumes that the diffusion rate in the gut system, k_g, is a fix constant, and there is no time delay between portal and arterial blood. It is not a priori known how these assumed factors degrade the accuracy of estimated DIF and flow. Moreover, tissue TACs from PET images convey some degree of noise, and the accuracy of the estimated input function might depend on either the degree of noise, or the applied number of tissue TACs, or both. A simulation study was designed to reveal the influence of the above elements on the accuracy of the current method.

To this purpose, we selected one arterial curve from one of the present experiments. First, a portal input curve was created by assuming k_g=0.5/min, corresponding to the estimated mean in all animals. The combination of these arterial and portal vein curves was treated as the 'true DIF'. In the present experimental study, the average of activity concentrations in an area of the summed image was distributed with a 20% range around the mean for the whole liver, and this percentage was independent of the size of the selected areas in regions >50 pixels. This supports the assumption that flow values in the liver distribute around a 20% range around a mean of arterial flow of 15 ml/min/100 g [22]. Thus, by assuming ten values of f_a as 13, 13.5, 14, 14.5, 15, 15, 15.5, 16, 16.5, and 17 ml/min/100 g, and ratio $r(=f_p/f_a)$=6 [22], one set of ten hepatic tissue TACs was generated from the true DIF using Eq. 6.

The propagation of an error in k_g and delay time to blood flow estimation was simulated. The sequence of steps in this procedure is simplified in Fig. 2a and b. For k_g, simulated portal input curves were created from the selected arterial curve by changing k_g from 0.35 to 0.65/min for error simulation in k_g, and combinations of the arterial and simulated portal vein curves were used as the simulated DIF. Sets of tissue TACs were generated from these simulated DIFs, with the same assumptions of f_a and r as given above. In turn, each set for each k_g was used to back-estimate DIF (arterial and portal components), fixing k_g as 0.5/min in this process as presented above. Finally, f_a and f_p were calculated from estimated DIFs for each k_g by the Gauss–Newton non-linear fitting method in the interactive modeling and data analysis system called PyBLD (http://homepage2.nifty.com/peco/pybld/pybld.html) [5] using Eq. 4. For delay time, simulated portal input curves were created from the selected arterial curve by shifting the time from 0 to 10 s, and combinations of the arterial and simulated portal vein curves were used as the simulated DIF. Sets of tissue TACs were generated as above. In turn, each set for each delay time was used to back-estimate DIF fixing time delay as 0.0 s. Finally, f_a and f_p were calculated from estimated DIFs for each delay time. Mean of percent difference between computed and assumed ('true') flow values are presented as a function of k_g and delay time.

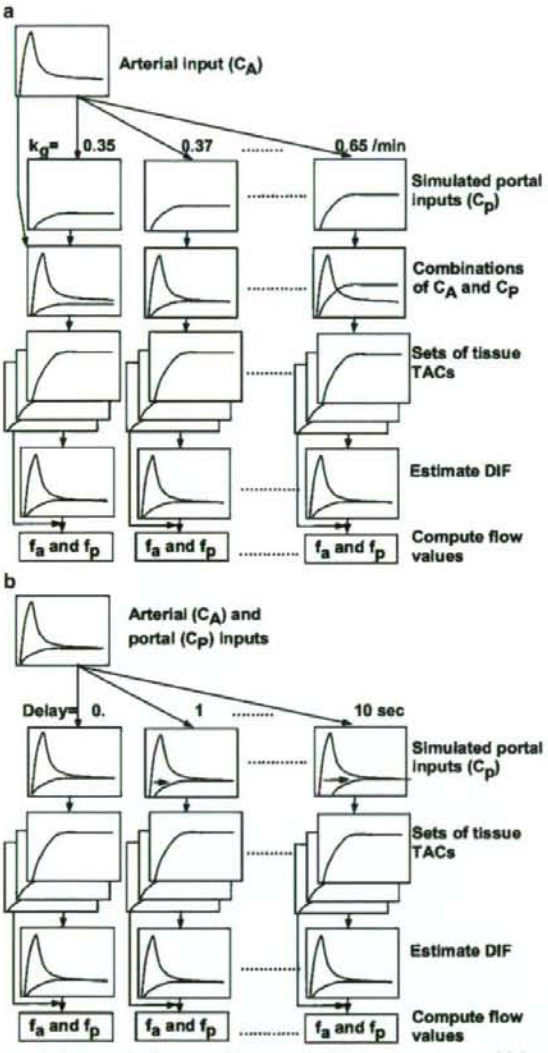

Fig. 2 Schematic diagram of the procedure to analyze error sensitivity in hepatic arterial (f_a) and portal flow (f_p) values against assumed k_g (**a**) and time delay (**b**). Portal input curves were created by changing the value of k_g from 0.35 to 0.65/min in (**a**) and by shifting the time from 0 to 10 s in (**b**), respectively, and combinations of the arterial (C_A) and simulated portal (C_P) curves were used as the simulated dual input functions (*DIF*). Sets of tissue time–activity curves (*TAC*) were generated from these simulated DIFs by assuming ten values of f_a from 13 to 17 ml/min/100 g. In turn, each set of tissue TACs was used to back-estimate DIF fixing k_g as 0.5/min and time delay as 0.0 s. Finally, f_a and f_p were calculated from estimated DIFs for each k_g and delay time

To analyze the influence of noise versus number of TACs on the accuracy of the method was explored. As shown by Edward et al. [7], as the noise on tissue TACs increased, the standard deviation of uptake ratio of tracer increased; as more regions were used, the standard deviation tended to decrease. However, if the number of TACs is larger, the noise on tissue is also large and vice versa. Our simulation was intended to reveal an optimal number of tissue TACs to be extracted from the whole region of the liver. The procedure is summarized in Fig. 3. First, tissue TACs with noise were generated as follows: Gaussian noise at peak was imposed on the set of ten hepatic tissue TACs generated above. Two levels of noise were introduced, corresponding to 10% and 20% of counts at the level of the peak and 10% and 20% each of the square root of counts at the other points. This procedure was repeated 100 times and 100 sets of noisy tissue TACs, embracing a total of 1,000 pixels obtained. Next, the ith set of tissue TACs in kth frame with f_a defined as $C_{fa}^{i,k}$ were summed for same f_a as

$$\overline{C}_{fa}^{k} = \frac{1}{N_T}\sum_{i}^{N_T} C_{fa}^{i,k} \tag{7}$$

where N_T indicates the summed number of tissue TACs and corresponds to the summed number of pixels. N_T were set to 5, 10, 20, 50, 100, and 200, corresponding to a number of tissue TACs (N_{tis}) of 200, 100, 50, 20, 10, and 5, respectively. Here, when N_T was 200, the 100 tissue TACs were summed as N_T=100 and additionally combinations of f_a=13 and 13.5, 14 and 14.5, 15 and 15, 15.5 and 16, and 16.5 and 17 ml/min/100 g were summed. For each N_{tis} and

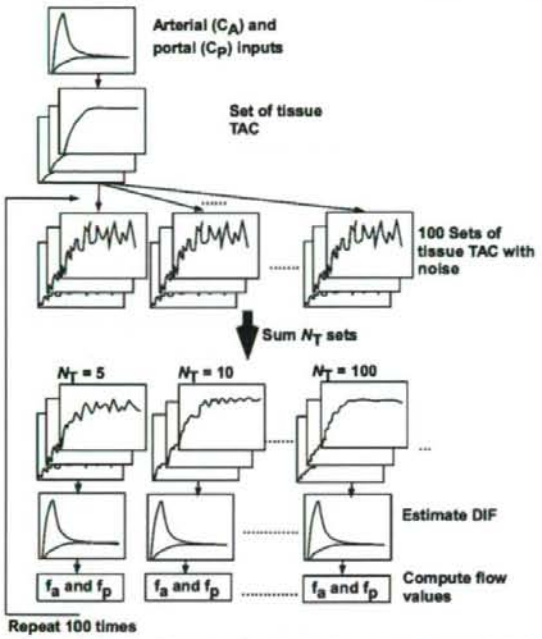

Fig. 3 Schematic diagram of the procedure to analyze statistical accuracy of hepatic arterial (f_a) and portal flow (f_p) values against noise on tissue curves. First, tissue time–activity curves (*TAC*) with noise were generated by imposing Gaussian noise on the set of ten hepatic tissue TACs. This procedure was repeated 100 times, and 100 sets of noisy tissue TACs were obtained. Next, the N_T (=5, 10, 20, 50, 100, and 200) sets of tissue TACs with the same flow value were summed. For each N_T, dual input function (*DIF*) was estimated. Then, arterial (f_a) and portal blood flow (f_b) values were computed using estimated DIF and tissue TACs. This procedure was repeated 100 times

each level of noise, DIF was estimated, as described. Then, arterial and portal vein blood flow values were computed as above, using estimated DIF and tissue TACs with f_a of 15 ml/100 g/min. This procedure was repeated 100 times, and the bias and deviation in values of arterial and portal vein flow results were calculated. Their bias and deviation was presented as a function of N_{tis}.

Experimental study

PET experiment

Fourteen pigs under anesthesia with weight 30.0±1.1 kg were studied. Data on glucose metabolism in these animals have been previously reported [13, 14]. Animals were deprived of food on the day prior to the study at 5:00 pm. Anesthesia was induced with ketamine (1.0 g) into neck muscles and maintained by ketamine and pancuronium (total of 1.5 g and 40 mg, respectively) administered intravenously during the experiment. Animals were intubated through a tracheostomy, and their respiration was controlled by a ventilator providing oxygen and normal room air (regulated ventilation, 16 breaths per minute). Catheters were inserted into the carotid artery for arterial blood sampling and the femoral vein for administration of $H_2{}^{15}O$. Splanchnic vessels were accessed by sub-costal incision; after dissection of the hepato-gastric ligament, purse string sutures were allocated to allow catheter insertion via a small incision in the portal vein. A catheter was inserted directly in the portal vein for portal vein blood sampling. Ultrasound-based flow-probes (Medi-Stim Butterfly Flowmeter, Medi-Stim AS) were placed around the portal vein and hepatic artery to determine blood velocity in each vessel. The diameter of the hepatic artery and portal vein were measured off-line from B-mode ultrasound images acquired using an Acuson Sequoia 512 mainframe with a 13-MHz B-mode linear array transducer. The area of the vessel was calculated assuming circular shape. Then, blood flow was obtained for each vessel during the PET scans. The surgical access was closed, and the distal catheter extremities were secured to the abdominal surface to avoid tip displacement. The animals were then transported to the PET center for tracer administration, liver imaging, and blood sampling. Vital signs, blood pressure, and heart rate were monitored throughout the study.

PET acquisition was carried out in 2D mode using an ECAT 931-08/12 scanner (CTI Inc, Knoxville, TN, USA) with a 10.5-cm axial field of view and a resolution of 6.7 mm (axial)×6.5 mm (in-plane) full width at half maximum. After transmission scan for attenuation correction, the dynamic scan was started after the injection of $H_2{}^{15}O$ (274 MBq, 30-s bolus injection), consisting of 20 frames with gradually increasing individual durations (6×5, 6×15, and 8×30 s).

During PET scanning, blood was withdrawn continuously from the carotid artery and portal vein through catheters (1.4 mm in inner diameter; length of tube was 900 mm to the detector and 60 mm in the detector sensitive region) by using a peristaltic pump (Scanditronix, Uppsala, Sweden) with a withdraw speed of 6 ml/min. Radioactivity concentrations in blood were measured with a BGO coincidence monitor system. The detectors had been cross-calibrated to the PET scanner via ion chamber [26].

At the end of the experimental period, animals were sacrificed by potassium chloride injection and anesthetic overdose, the abdominal cavity was rapidly accessed, and the whole liver was explanted and weighed and its volume was measured by water displacement; liver density was calculated as the ratio of organ weight-to-volume to derive the ultrasound-based flow to PET-equivalent unit (i.e., flow per unit of tissue volume).

The protocol was reviewed and approved by the Ethical Committee for Animal Experiments of the University of Turku.

Data processing

Dynamic sinogram data were corrected for dead time in each frame in addition to detector normalization. Tomographic images were reconstructed from corrected sinogram data by the median root prior reconstruction algorithm with 150 iterations and Bayesian coefficient of 0.3 [1]. Attenuation correction was applied with transmission data. A reconstructed image had 128×128×15 matrix size with a pixel size of 2.4 mm×2.4 mm and 6.7 mm with 20 frames.

Measured arterial and portal vein blood TACs were corrected for physical decay and dispersion [11] as τ=2.5 s, which was experimentally obtained and usually applied in our center. The arterial TAC corrected for decay and dispersion was then corrected for delay by fitting to a whole-liver tissue TAC [12]. The arterial curve obtained, $C_a(t)$, was used as the measured arterial input function. Then, the portal vein curve, corrected for dispersion (τ= 2.5 s) and delay with the same delay time for arterial TAC, $C_P(t)$, was fitted according to the following equation:

$$C_P(t) = k_g C_a\left(t + \Delta t_p\right) \otimes e^{-k_e\left(t+\Delta t_p\right)} \quad (8)$$

to obtain k_g and to account for the appearance time (Δt_p seconds) via the gut system. Obtained measured curves were directly fitted with Eqs. 1 and 2 to examine adequacy for a usage of model functions.

A region of interest (ROI) was placed on the whole region of the liver in a summed image and subsequently divided plane-by-plane into sub-regions of 700 pixels each, corresponding to 11–22 sub-regions. Sub-regions were created by extracting pixels firstly from horizontal then vertical directions inside the whole ROI in each slice. Each sub-region consisted of a single area with the same number of pixels. Tissue TACs in the sub-regions were extracted from dynamic images. Then, DIF was estimated according to the procedure introduced above. In the first step, initial values and boundary conditions for the non-linear fitting (PAW environment) for each parameter were 20,000 between 0.0000002 and 200,000,000 Bq/ml for A, 5 between 2 and 20 ml/min for $K_e(1+\alpha)$, 1 between −10 and 100 s for t_1, 20 between 1 to 60 s for t_2-t_1, 20 between 1 and 100 ml/min/g for f_a, 100 between 1 and 400 ml/min/g for f_b, and 0.05 between 0 and 1 ml/ml for V_0. In the second step, S^2 value in Eq. 6 was minimized, and the image-based input function was obtained. Areas under the curves (AUC) for measured and image-based inputs were calculated for 0 to 180 s. Their percent difference was calculated.

Perfusion values f_a and f_p were calculated by non-linear Gauss–Newton fitting method (PyBLD environment). Results obtained with the new technique were compared with (a) those obtained with the measured input function and (b) the ones from our independent reference method, i.e., ultrasonography, after their normalization to the organ volume to derive PET-equivalent units.

Statistical analysis

Data are shown individually or as mean±SD. The Student's paired t test was used for intra-individual comparisons of flow values. Regression analyses were performed according to standard techniques. A $p<0.05$ was considered to be significant. Differences between the flow values were calculated as $(f_X-f_Y)/f_X$ where f_X and f_Y are flow values from the non-invasive method and from the measured input or ultrasonography, respectively, and plotted in Bland–Altman plot [3].

Results

Simulation study

The biases in values of arterial, portal vein, and total blood perfusion due to a fixed k_g and delay time are presented in Fig. 4a and b as a function of the value of k_g and delay time, respectively. The error in total flow results did not exceed 10% for a ≤20% (i.e., 0.4–0.6 min^{-1}) difference between the fixed and the assumed (true) k_g and for a <10-s time delay.

The influence of noise and number of tissue TACs, i.e., the bias and deviation on both arterial and portal blood flow values, showed to be minimal for a number of tissue TACs of 10 to 20 at both noise levels (Fig. 5). As shown in Fig. 5, if the number of tissue TACs is increased, noise on each curve for input estimation becomes larger. On the other hand, a smaller number of tissue TAC corresponds to less information from tissue TAC in terms of variation of flow values. This result suggested that the optimal number of tissue TACs to be applied to preserve accuracy is in the above range, which is independent of the two noise levels. Among the five parameter composing the model input functions, the three parameters t_1, t_2, and r_a were determined with same accuracy, i.e., both the difference and deviation in those values were less than 1 s for t_1 and t_2 and 5% for r_a, respectively, for the noise level of 10%, independent of the number of tissue TACs. Bias and deviation of the remaining two parameters A and $K_e(1+\alpha)$ depended on the number of tissue TACs following the same tendency as the bias and deviation on blood flow values, as described above.

Experimental study

Reconstructed images are shown in Fig. 6, together with divided sub-regions. In the first step of our procedure, the

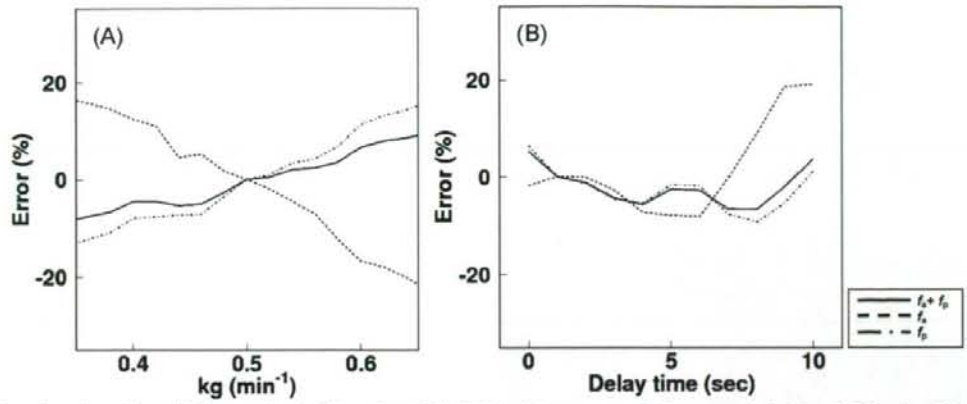

Fig. 4 Error in values of arterial (f_a), portal vein (f_p), and total (f_a+f_p) blood flow propagated from error in k_g (**a**) and delay time (**b**)

obtained value of t_1 from TACs extracted from sub-regions overlapping the vena cava (e.g., lower sub-region at upper left side image in Fig. 6) was 10 to 13 s earlier than the mean, and these TACs were omitted from further processing. The estimated t_2-t_1 was 27±3 s, which was similar to the tracer administration duration.

Figure 7 shows the curves of the model arterial and portal input functions (Eqs. 1 and 2) directly fitted to measured curves. The model functions for those were superimposable to measured curves, although both modeled curves slightly overestimated at the late times. This result suggested that the model function was almost adequate to use for the estimation of input.

The mean±SD of k_g was 0.497±0.153 ml/min/g and that of Δt_p was 0.7±5.1 s obtained by fitting the portal TAC using arterial TAC by Eq. 8.

Estimated, image-derived arterial and hepatic input functions were almost superimposable to the measured curves (Fig. 8). The mean±SD and range of difference of AUCs were −3.15±8.73% ranging from −13.5% to 17.9% and 1.47±8.87% ranging from −13.5% to 10.2% for arterial and portal input functions, respectively. The coefficient of variation of the estimated flow ratio between artery and portal vein in the first step across sub-regions was 26±9%. The mean±SD of that ratio across subjects was 0.15±0.07 and those from ultrasonography was 0.16±0.06, and paired t test showed no significant difference between them. This suggests supporting the assumption that the ratio between arterial and portal input defined in Eq. 5 relates to the flow values.

The Bland–Altman plot between values of hepatic arterial, portal, and total perfusion, as estimated by using the image-derived versus the measured blood curves, is shown in Fig. 9. This plot demonstrates a small overestimation by image-derived method with a bias of 0.01 and 0.07 ml/min/g for arterial and portal flow, respectively, and that 0.08 ml/min/g for total flow. Respective regression lines were the following: y=0.00+1.09 x (r=0.97, p<

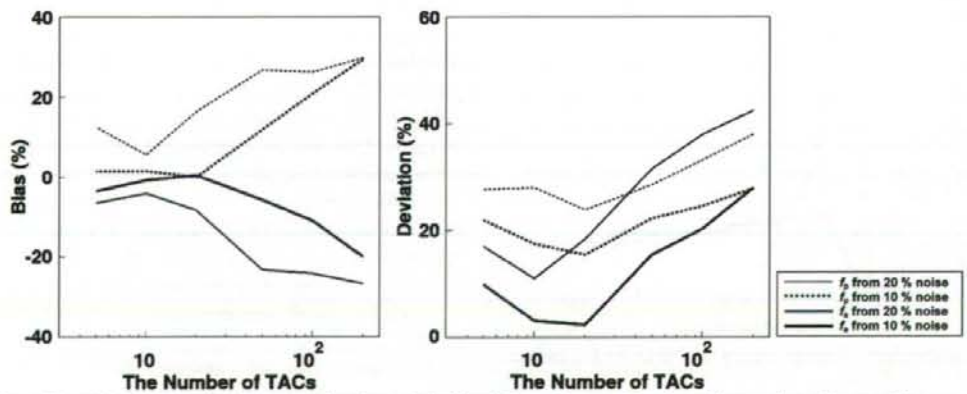

Fig. 5 Bias (*left*) and deviation (*right*) in the arterial and portal vein blood flow values as a function of the number of time–activity curves applied to the estimation of the input function

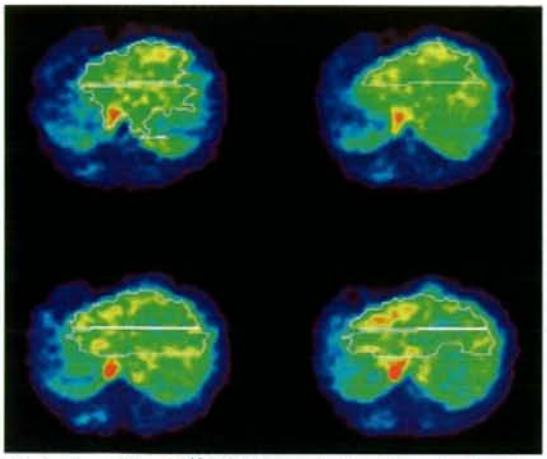

Fig. 6 View of liver $H_2{}^{15}O$ PET images in four slices and sub-regions (*solid line*). The small area with high activity levels on the mid-right and mid-left side of the image corresponds to the vena cava and aorta, respectively

0.001), $y=0.05+1.02\ x$ ($r=0.87$, $p<0.001$), and $y=0.02+1.06\ x$ ($r=0.90$, $p<0.001$). Paired t test showed no significant difference between the methods. Differences were $-6.8\pm20.0\%$, $-4.9\pm14.3\%$, and $-5.8\pm15.6\%$ for arterial, portal, and total blood flow values, respectively.

The Bland–Altman plot between values of hepatic arterial, portal, and total perfusion, as estimated by using the current method versus ultrasonography, is given in Fig. 10. This plot demonstrates an overestimation by image-derived method with a bias of 0.02 and 0.22 ml/min/g for arterial and portal flow, respectively, and that 0.24 ml/min/g for total flow. Respective regression lines were the following: $y=0.06+0.69\ x$ ($r=0.69$, $p=0.12$), $y=0.41+0.98\ x$ ($r=0.54$, $p=0.025$), and $y=0.24+0.97\ x$ ($r=$

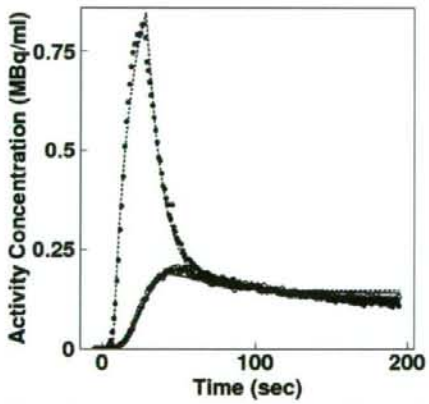

Fig. 7 Time–activity curves representing the arterial (*broken line*) and portal (*solid line*) model input functions (Eqs. 1 and 2) in comparison with the measured arterial (*black circles*) and portal (*open circles*) input functions

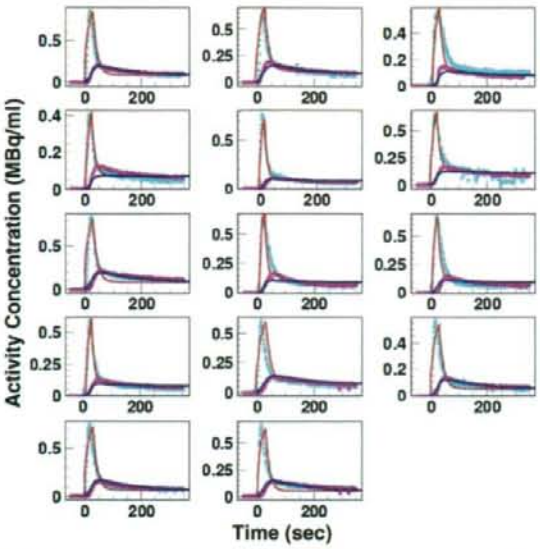

Fig. 8 Estimated arterial (*red line*) and portal vein (*blue line*) input functions from PET images and their comparison with measured arterial (plot in *light blue*) and portal input (plot in *pink*) functions

0.60, $p=0.022$). Again, paired t test showed no significant difference between the methods. Differences were $3.6\pm52.0\%$, $15.5\pm31.3\%$, and $16.9\pm33.0\%$ for values of arterial, portal, and total blood flow, respectively.

The total flow values ranged from 0.5 to 2 ml/min/g in the animals (Figs. 9 and 10). However, only two out of 14 showed smaller values of 0.5 ml/min/g (i.e., approximately 500 ml in the whole organ), which is still physiologically reasonable, while the great majority clustered between 1 and 2 ml/min/g.

Discussion

In the current work, we developed and validated a method to estimate the two components of the hepatic dual input function from liver $H_2{}^{15}O$ PET images and quantify hepatic perfusion. Computer simulations were used to evaluate the influence of assumptions, noise in raw data, and number and size of the regions of interest to be used in the analysis. After demonstrating that k_g can be assumed within a 20% range by introducing a negligible error in perfusion estimates and that 10–20 regional time–activity curves appear optimal, the method was validated experimentally by showing its coherence with measured blood tracer levels and with liver perfusion results obtained by an independent technique.

The current approach estimated the hepatic arterial and portal input functions from multiple tissue curves to calculate respective and total organ perfusion. A high